Confinement induces actin flow in a meiotic cytoplasm

Mathieu Pinot[a], Villier Steiner[b], Benoit Dehapiot[c], Byung-Kuk Yoo[b], Franck Chesnel[c], Laurent Blanchoin[d], Charles Kervrann[e], and Zoher Gueroui[b,1]

[a]Institut Curie, Unite Mixte de Recherche 144 Centre National de la Recherche Scientifique, 12 rue Lhomond, 75005 Paris, France; [b]Ecole Normale Supérieure, Département de Chimie, Unite Mixte de Recherche 8640 Centre National de la Recherche Scientifique-ENS-Université Pierre et Marie Curie, 24, rue Lhomond, 75005 Paris, France; [c]Centre National de la Recherche Scientifique/Unite Mixte de Recherche 6290, Institut de Génétique et Développement de Rennes—Université de Rennes I—IFR140, 2 avenue du Professeur Léon Bernard, 35043 Rennes Cedex, France; [d]Institut de Recherches en Technologies et Sciences pour le Vivant-Laboratoire de Phyiologie Cellulair`e and Végétale, Centre National de la Recherche Scientifique-Commissariat à l'énergie atomique-UJF, Grenoble 38054, France; and [e]INRIA, Centre de Rennes—Bretagne Atlantique, Serpico Team, Campus de Beaulieu, 35042 Rennes Cedex, France

Edited by Claudia Veigel, Ludwig-Maximilians-Universität München, München, Germany, and accepted by the Editorial Board June 4, 2012 (received for review January 4, 2012)

In vivo, F-actin flows are observed at different cell life stages and participate in various developmental processes during asymmetric divisions in vertebrate oocytes, cell migration, or wound healing. Here, we show that confinement has a dramatic effect on F-actin spatiotemporal organization. We reconstitute in vitro the spontaneous generation of F-actin flow using *Xenopus* meiotic extracts artificially confined within a geometry mimicking the cell boundary. Perturbations of actin polymerization kinetics or F-actin nucleation sites strongly modify the network flow dynamics. A combination of quantitative image analysis and biochemical perturbations shows that both spatial localization of F-actin nucleators and actin turnover play a decisive role in generating flow. Interestingly, our in vitro assay recapitulates several symmetry-breaking processes observed in oocytes and early embryonic cells.

cytoskeleton | self-organization | symmetry breaking

Actin-based dynamics are observed at different stages of embryonic and adult cell life and participate in various essential processes, such as cytokinesis (1), asymmetric divisions in vertebrate oocytes (2–4), cell migration (5, 6), or wound healing (7–9). Recent findings have highlighted key functional roles of cytoplasmic F-actin in oocytes and eggs, such as spindle positioning in mouse occytes (2–4, 10, 11) or the chromosome congression and intracellular transport in starfish (12, 13). The generation and maintenance of such cellular functions are often correlated with symmetry breaking and spatiotemporal reorganization of F-actin assembly (14, 15). In vitro assays had provided important contributions in the understanding of the spatial organization and dynamics of functional F-actin structures (16–20). In addition, the effect of the geometry of boundary conditions on the cytoskeleton organization have been investigated using in vitro compartmentalization of cytoskeleton proteins (21–26) or using surface patterning techniques (27). *Xenopus* egg extracts had provided a powerful system to dissect mechanisms of many aspects of cell division in vitro and has been extensively used to study bipolar spindle assembly (28–30). F-actin and microtubule interactions were examined in interphase extracts (31) and actomyosin dynamic has been linked to cell cycle regulation using egg extracts (32). However, despite these progresses, the spatiotemporal dynamics of cytoplasmic F-actin network, and in particular of actin flows, are still unclear. In order to gain some insights into the generation and maintenance of cytoplasmic F-actin flow dynamics, we have developed an in vitro system capturing the spatial organization of cytoskeleton filaments within a confined geometry that mimics the cellular environment. This system, based on the cellular reconstitution by confinement of *Xenopus* cytoplasmic extracts, is used to examine functional *Xenopus* egg extracts in a confined environment while keeping some of the advantages of the cell extracts: biochemical manipulations, straightforward control over cell cycle progression, and very good optical properties in regard to the difficulty to image large embryonic cells. More precisely, we generate femto-liters of cytoplasmic *Xenopus* egg extracts confined within emulsion droplets stabilized at the boundary with a phospholipid monolayer or an amphiphilic polymer. F-actin spatial organization in confined geometry contrasts drastically from bulk. Whereas bulk F-actin organized in a random network, symmetry in F-actin organization is broken in confined geometry. F-actin self-organized into a contractile ring-like structure surrounded by an actin cloud with the presence of a flow of F-actin. To decipher the mechanisms involved in this process, we quantify the dynamical behavior of F-actin flow. Observations of F-actin dynamics within droplets showed network remodeling with both filaments nucleation at the boundary condition and filament transport directed radially inward. Inhibition or modification of F-actin polymerization dynamics by cytochalasin D or phalloidin alters the flow and symmetry breakings. Addition of a domain of Scar (Scar-WA/pWA), a cellular activator of Arp2/3 that contains both the actin and Arp2/3 binding motifs, stimulates bulk nucleation of F-actin and impedes symmetry breakings and flow dynamics. We finally investigate the influence of the cell cycle state and find that F-actin dynamics in confined interphase extracts show a behavior qualitatively similar to those observed in confined metaphase extracts. Inhibition of myosin-II activity suggests that contractile elements participate in flow dynamics but are not essential to flow maintenance.

Results

Symmetry Breaking in F-actin Organization Within Droplets. To observe F-actin network organization in bulk cell extracts, we have supplemented metaphase II-arrested *Xenopus* oocyte extracts with 50 nM of Alexa488-conjugated phalloidin. After few minutes of incubation at room temperature of such bulk extract, we observed an interconnected network of F-actin filling the entire extract volume (Fig. 1*A*). F-actin fibers organized into meshworks that were either homogeneous in space or that could exhibit a spatial heterogeneity in F-actin concentration (Fig. 1*A*, *Left* and *Right*, respectively).

To investigate the dynamics of F-actin network in a confined environment mimicking the cell context, we entrapped functional

Author contributions: M.P. and Z.G. designed research; M.P., V.S., B.D., B.-K.Y., C.K., and Z.G. performed research; F.C., L.B., and C.K. contributed new reagents/analytic tools; M.P., V.S., B.D., B.-K.Y., F.C., L.B., C.K., and Z.G. analyzed data; and M.P. and Z.G. wrote the paper.

The authors declare no conflict of interest.

This article is a PNAS Direct Submission. C.V. is a guest editor invited by the Editorial Board.

[1]To whom correspondence should be addressed. E-mail: zoher.gueroui@ens.fr.

This article contains supporting information online at www.pnas.org/lookup/suppl/doi:10.1073/pnas.1121583109/-/DCSupplemental.

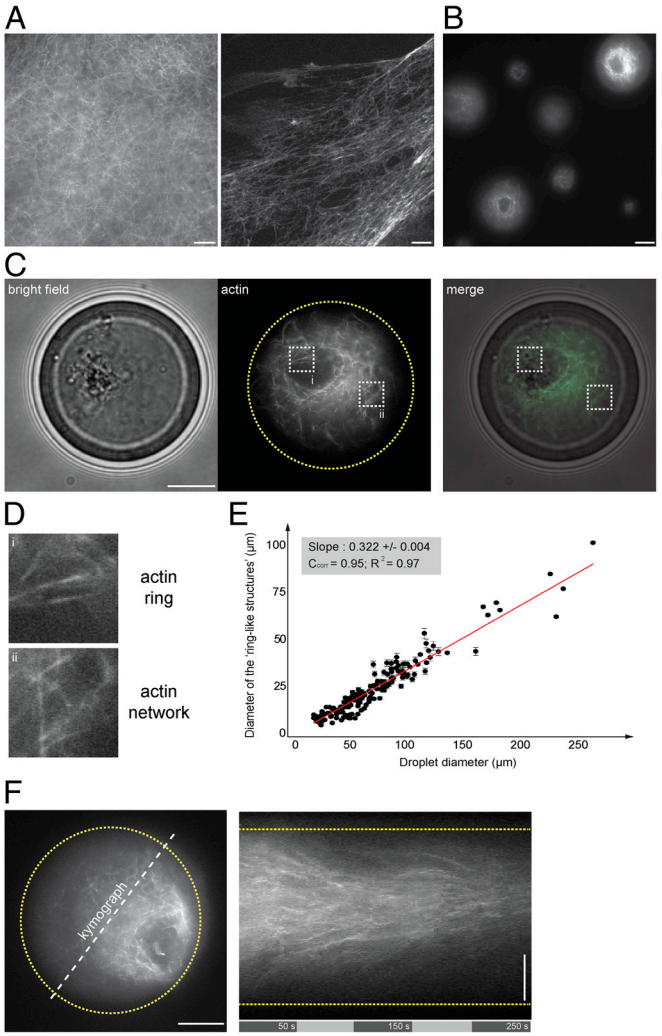

Fig. 1. Symmetry breaking of confined F-actin network. (*A*) Fluorescent observation of F-actin network (in presence of Alexa488-conjugated phalloidin) generated in bulk extracts (5 min incubation). (*B*) Fluorescent observation of F-actin network within extract-in-oil droplets. (*C*, *D*) Bright field and fluorescent observations of F-actin network confined within a 34 µm-diameter droplet. (*D*) Actin filaments organized in a ring-like structure asymmetrically positioned within the droplet and surrounded by an actin cloud (actin network). (*E*) Plot of the ring-like structure diameter as a function of the droplet diameter shows a linear correlation between the ring and the droplet diameter. Quantifications of the ring diameters were performed by extracting a plot profile of the fluorescent structure. The droplet diameter was measured using bright field illumination. We estimated the precision of such measurements to 1 µm. (*F*) Representative kymograph illustrating the directional flow dynamics of F-actin network within a 40 µm-diameter droplet. Scale bars, 10 µm.

cytoplasm using in vitro compartmentalization methods. These approaches were successfully applied to confine purified proteins (21, 25, 33), and we recently demonstrated that *Xenopus* extracts retain their capability of assembling microtubules when confined within droplets (26, 34). We generated droplets of *Xenopus laevis* egg extracts dispersed in mineral oil (26, 34). This method allows the formation of a large number of spherical droplets with diameters ranging from 10 to 200 µm (Fig. 1*B*). F-actin spatial organization in confined geometry contrasted drastically from bulk. After few minutes of incubation, the majority of the droplets (more than 90%) contained bright fluorescent actin bundles organized in a very distinct pattern than the ones observed in unconfined conditions (bulk). In droplets, F-actin filaments self-organized in highly stereotyped structures evoking a ring-like structure that is surrounded by an actin cloud (Fig. 1 *C* and *D* and Fig. S1*A*). The observation of several droplets in a same field of view showed that the ring-like structures localized randomly in space within droplets (Fig. 1*B* and Fig. S1*B*).

To study the role of the confinement size on actin pattern organization, we measured the apparent diameter of the ring-like structures as a function of the droplet diameter (Fig. 1*E*, 20 to 250 µm, 169 droplets, nine independent experiments). We found a linear correlation between the ring and the droplet diameter, suggesting a scaling of F-actin self-organization with the droplet size. For smaller droplets, we found that 40% of the droplets exhibit a ring-like structure, whereas 60% failed in organizing a ring-like structure (Fig. S1 *C* and *D*, 50 droplets, and seven independent experiments). Altogether, these data suggest that F-actin self-polarized and accumulated asymmetrically within droplets in contrast with unconfined environment (bulk experiments).

Dynamics of F-actin Network: Spontaneous Flow Generation Within Droplets. Interestingly, 1–3 min after the initiation of the F-actin nucleation, we observed the spontaneous generation of F-actin flow within droplets (Fig. 1*F* and Movies S1 and S2). Closer observations of F-actin dynamics within droplets showed network remodeling with both filament nucleation at the vicinity of the boundary and filament transport directed radially inward (Fig. S2*A*). In addition, bright field observations permitted to distinguish a local enrichment of cytoplasmic materials entrapped within the dense F-actin meshwork (Fig. 1*C*). This suggests that F-actin flow may convey cytoplasmic materials through a process that could be linked to F-actin based transport. To provide some insights to this hypothesis, we monitored cytoplasmic material movement during the formation of F-actin ring-like structures using fluorescently labeled beads as passive markers (Fig. S1*E*). The beads entrapped by the meshwork of filaments eventually accumulated within the ring-structures. These experiments are reminiscent to those recently described in starfish oocytes, where directional transport by F-actin meshwork was proposed to guide passive large objects by steric trapping (13), or where F-actin dynamics were linked to cytoplasmic streaming in mouse oocytes (10). Finally, in some observations, the ring-like structure position moved randomly within the droplet space (Fig. S2*B* and Movie S2). Altogether these observations suggest that F-actin flow in droplet is mainly directed radially inward, with a centripetal direction from the periphery of the droplet to a convergent area.

In order to get some insights on the mechanisms involved in F-actin flow generation, we first characterized the dynamics behavior of the meshwork in bulk and in droplets. We used optical flow methods to extract the spatiotemporal positions of nodes or bright filaments of the F-actin network (Fig. 2, *SI Materials and Methods*). For instance, we reported on Fig. 2*A* representative examples of the displacement fields of trajectories as a function of time. Computation of the velocity field and vector flow orientation showed variability in velocity distribution and orientation of bulk F-actin networks. We have reported the analysis of approximately 600 trajectories on Fig. S2*C* (six independent experiments, mean = 44 ± 13 nm s^{-1}). More generally, about 60% of experiments exhibited F-actin dynamics associated with a mean velocity of about 10–20 nm s^{-1}, whereas about 40% were characterized by a velocity reaching approximately 50–80 nm s^{-1} (40 independent experiments). In addition, orientation of F-actin displacement fields could be either similar or distinct throughout the same field of observation (examples 1, 2 and 3, 4, respectively). Both heterogeneity due to cell extract preparations and intrinsic variability of the mechanisms involved in F-actin dynamics may account for the variation observed.

Next, we quantified F-actin dynamics in a confined environment. Fig. 2*B* displays the displacement field of F-actin meshwork within a single droplet (approximately 30 trajectories). For this

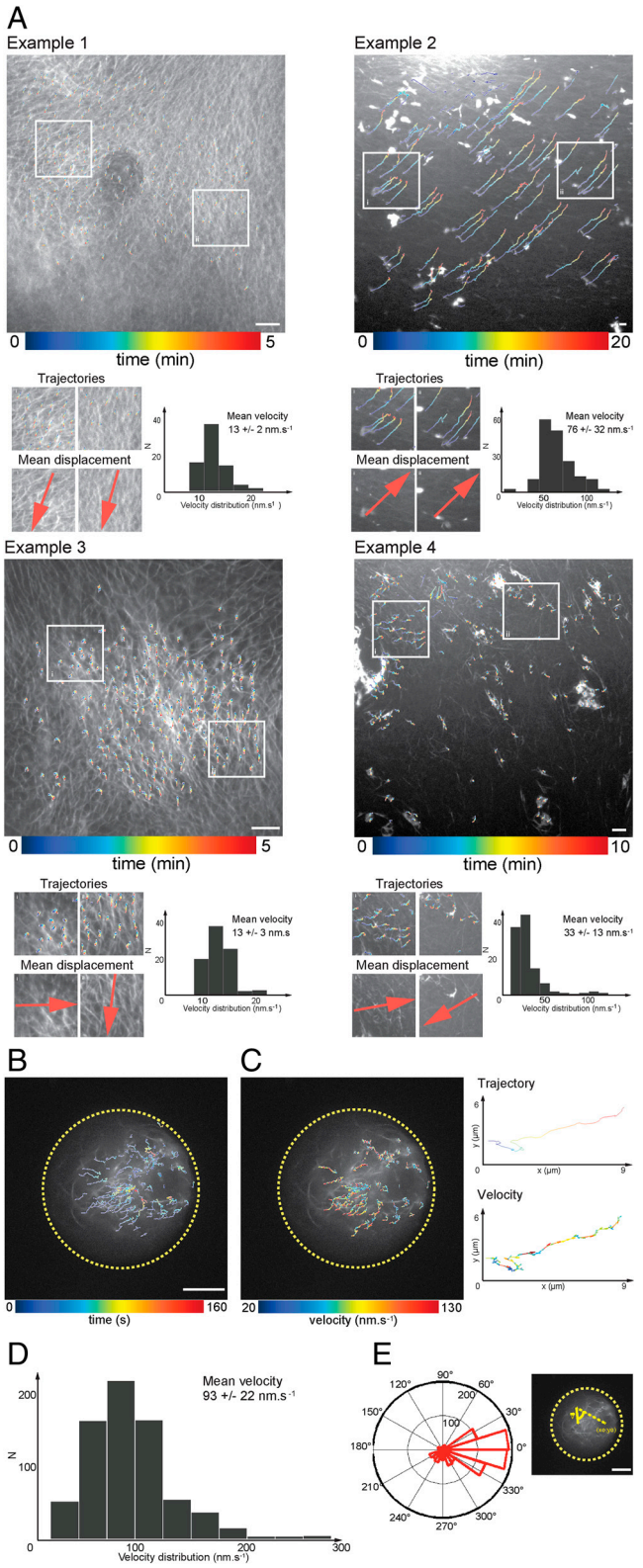

Fig. 2. F-actin spatiotemporal dynamics in bulk and within droplets: quantitative characterization of the flow velocity. (*A*) Displacement field of trajectories in bulk extracts shows variability in velocity distribution and orientation of F-actin network. (*B*) Displacement fields reveal a convergent flow toward the ring-like structure. (*C*) Velocity field amplitude distribution computed for trajectories tracked within a single droplet. (*D*) Histogram of mean velocities (mean = 93 ± 22 nm s^{-1}, N = 15 experiments, 700 trajectories, and 20 droplets). (*E*) Angular orientation of tracked trajectories (N = 20 droplets, approximately 600 trajectories analyzed). Scale bars, 10 μm.

example, we computed the velocity field and extracted the velocity distribution, the mean velocity (90 ± 40 nm s^{-1}) and the angular orientation of tracked trajectories (Fig. S2*D*). The analyses performed over 20 droplets showed that F-actin dynamics were of the same magnitude, illustrating a common behavior between single droplets. The majority of the filaments were initially localized at the droplet periphery and moved toward the ring region with a mean velocity of 93 ± 22 nm s^{-1} (Fig. 2*D*, approximately 700 trajectories, 20 droplets, and 15 independent experiments). Both angular distributions of the trajectories and deviation of the mean orientation to the center of the ring-like structure showed that F-actin movements are persistent over 5–10 μm toward the center of the structure (Fig. 2*E*, 15 droplets analyzed). Velocity fields along single trajectories are highly heterogeneous within droplets (Fig. 2*C*). For instance, the amplitude of the velocity along single tracked trajectories within droplets spans from approximately 20 nm s^{-1} to approximately 130 nm s^{-1}. These trajectories generally exhibit a rapid movement ("hopping") with distances ranging from 0.5 to 7 μm, with a mean hopping distance of 2.5 μm (Fig. S2*E*). These analyses show that the velocities measured in confined extracts are larger than the ones measured in unconfined extracts. A second difference between confined and bulk geometry relies on the presence of a convergent flow directed radially inward a ring-like structure under confinement, whereas no ring-like structure was observed in bulk. Interestingly, velocities in confined geometry are of the same magnitude of those measured for retrograde flows during cell migration, wound healing and actin-ring constriction during cytokinesis (6, 8, 35).

In Fig. 3*A* and Fig. S2*A*, we reported examples of F-actin nucleation occurring at the vicinity of the droplet boundary. Both time-evolution trace of the integrated intensity of the fluorescent signal and a kymograph representation demonstrate that F-actin production shows periodicity of approximately 100 s (Fig. 3*B*). These dynamics are reminiscent of F-actin waves or pulses observed in cytoplasm of *Xenopus* eggs (32, 36), in *Dictyostelium discoideum*, leukemic cells (37–39), and *Drosophila* germ band extension (40). Interestingly, in our system, the confinement geometry provided by the droplets defines the boundary conditions of actin nucleation activity (27). Several mechanisms may account for F-actin nucleation at the vicinity of the boundary. First, the recruitment of actin promoting factors such Arp2/3 by N-Wasp may be considered (1, 5). Indeed, the partial hydrophobic nature of the extract/oil interface composing the droplet boundary could induce a conformational change of N-Wasp leading to its activation and the recruitment of Arp2/3 complexes (41). Alternative mechanisms that may explain the generation of F-actin wave dynamics rely on theoretical models of stochastic nucleation/growth processes. They involved either treadmilling of filaments nucleated by Arp2/3 without requiring myosin-II activity (42) or a process of filament growth coupled to myosin-II contractility (32).

Fusion Process Between Two Self-Organized F-actin Assemblies Reveals that F-actin Networks are Dynamic and Adaptable Structures. One typical feature of F-actin organizations within droplets is that no more than one well-defined organization per droplet is observed. However, the coalescence of two adjacent droplets provided us a means to monitor the interactions of two organized F-actin structures evolving in the same micro-environment. On Fig. 3*C*, we have reported an example of two adjacent droplets that coalesced into one larger droplet with two actin ring-like structures that share the same cytoplasmic region and, thereby, interact with each other. Remarkably, within 2 min, the two F-actin structures started to remodel and fuse toward a single actin-based organization. We could isolate three events characterizing the fusion process: droplet fusion (Fig. 3*D*, *i*), network fusion (Fig. 3*D*, *ii*), and ring fusion (Fig. 3*D*, *iii*). After the droplet

fusion event, the two F-actin networks were separated by approximately 11 μm and the directionality and mean velocity of their dynamics were not modified. The two F-actin network structures started to interact and get closer, approximately 30 s after the droplet fusion. Interestingly, mean velocity measurements showed how F-actin dynamics drastically slowed down in a time window corresponding to the initiation of F-actin network interactions until the beginning of the network fusion (about 60 s). The last event corresponds to the fusion of the two rings structures to a single organization with one main centripetal flow. During this step, the mean velocity increased to reach approximately 140 nm s^{-1}, which is close to unperturbed flow dynamics. We monitored four additional fusion processes, and all recapitulated the steps described in Fig. 3*D* (Fig. 3*E*, second example). This adaptive or plastic behavior may be an outcome of the rapid turnover of actin through treadmilling and actin bundle fusion. This property is characteristic of biological self-organized organelles, such as the meiotic spindle or the Golgi that are maintained far from thermodynamical equilibrium (30, 43–45). It illustrates the architectural plasticity of the actin network in which actin turnover provides a structural feedback.

Effect of Actin Polymerization on F-actin Flow. To probe the role of the filament dynamics in the establishment of F-actin flow, we first monitored the spatiotemporal organization of F-actin networks in presence of increasing concentrations of cytochalasin D (0.1–5 μM). With 0.1 μM, 0.5 μM, and 1 μM, a cluster of small and bright filaments formed within the droplets (Fig. S3*A*). At these concentrations, we can still distinguish a very weak fluorescent signal of F-actin network flow. When using 5 μM, the bright F-actin clusters were still observed but without F-actin flow surrounding the organization. F-actin nucleation at the boundary was also abolished. Additional proof of the role of actin dynamics came from the stabilization of the filaments using phalloidin. Phalloidin (0.05 to 1 μM) added to the extract impeded actin network flow (Fig. S3*B*). Altogether, these results show that actin dynamics, such as treadmilling, are essential in the maintenance of F-actin flow.

Role of the Spatial Localization of F-actin Nucleation Sites. A clue to the origin of the F-actin flow comes from the spatial localization of F-actin at the vicinity of the droplet boundary. We designed an experiment to enhance F-actin nucleation homogeneously within the droplet bulk. We have supplemented the cell extract with a domain of Scar (Scar-WA/pWA), a cellular activator of Arp2/3 that contains both the actin and Arp2/3 binding motifs, to stimulate bulk nucleation of F-actin (46). Three concentrations were tested (0.5, 1.7, and 5 μM). With these conditions, we observed almost systematically a random meshwork of F-actin filling entirely the droplets (Fig. 4*A*). Scar-WA induced homogeneous growth of F-actin in the bulk droplet. Interestingly, neither F-actin flow nor actin ring-like structure was observed, contrast-

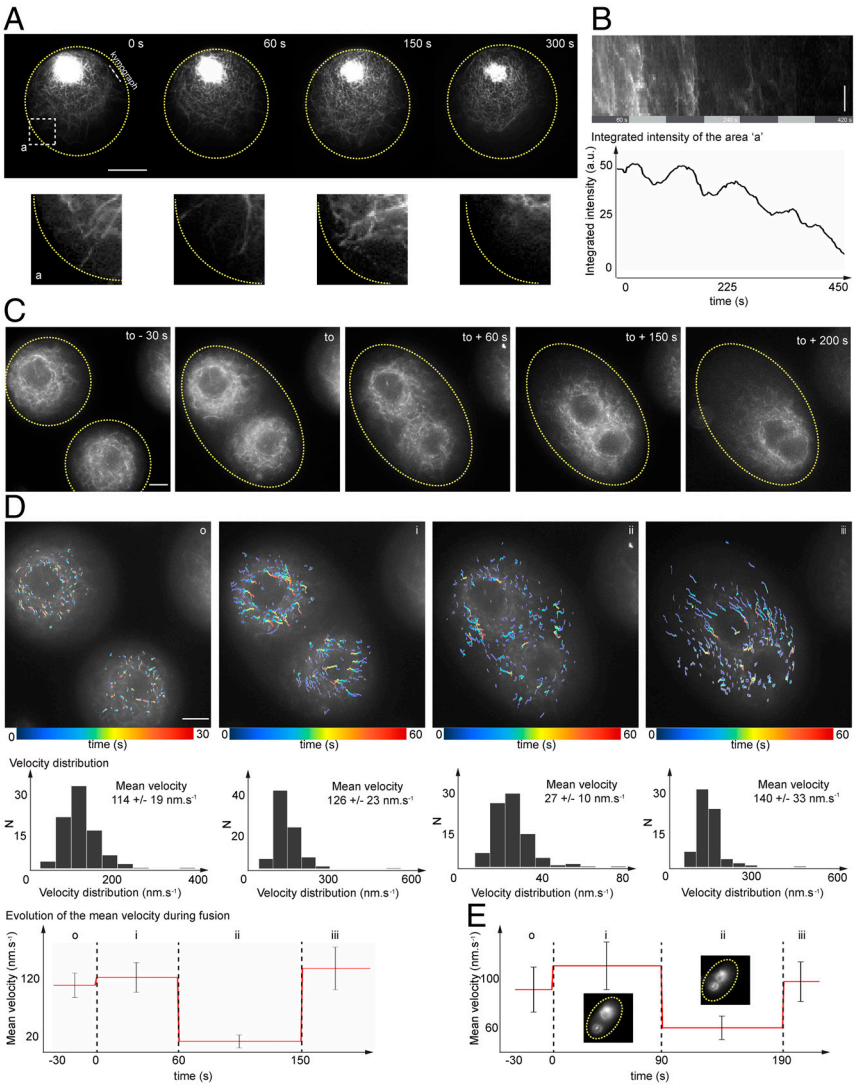

Fig. 3. Dynamical properties of the F-actin network: periodicity in F-actin production at the boundary and actin-based structure fusion. (*A*) Time series of F-actin production at the droplet boundary. (*B*) Kymograph representation and time evolution of the integrated intensity of a region of interest localized at the vicinity of the droplet boundary. F-actin production shows periodicity with a period of approximately 100 s. (*C*) Time series acquisitions of two droplets undergoing fusion. (*D*) Characterization of velocity distributions for three steps: (*i*) prior to droplet fusion, (*ii*) during F-actin network fusion, and (*iii*) during ring-like structure fusion. (*E*) Evolution of the mean velocity in a second fusion droplet event. Scale bars, 10 μm.

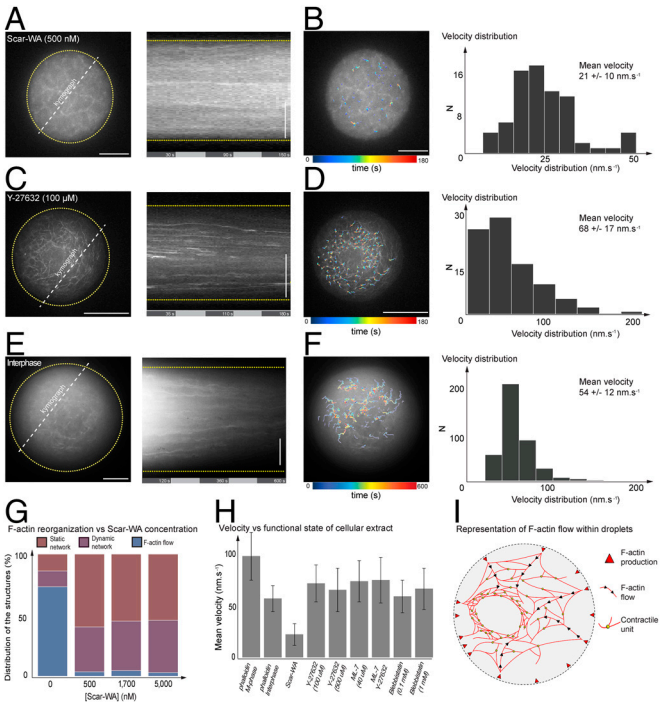

Fig. 4. Testing the role of the spatial localization of F-actin nucleation sites, the requirement of myosin II, and the regulation of the cell cycle in the generation of symmetry breaking and actin flow. (*A*) Kymograph of F-actin dynamics within droplet in presence of Scar-WA (500 nM). (*B*) Velocity field in presence of Scar-WA inhibitor (500 nM) and velocity distribution (N = 3 droplets, approximately 70 trajectories, mean = 21 ± 10 nm). (*C*) Kymograph of F-actin network in presence of Rho-Kinase inhibitor Y27632 (100 µM). (*D*) Velocity field of F-actin network dynamics in presence of Rho-Kinase inhibitor Y27632 (100 µM) and velocity distribution (N = 5 droplets, approximately 100 trajectories, mean = 68 ± 17 nm). (*E*) Kymograph of F-actin dynamics within droplet in interphase state. (*F*) Velocity field in interphase state and velocity distribution (N = 10 droplets, approximately 500 trajectories, mean = 54 ± 12 nm). (*G*) Histogram of events characterizing the network dynamic state for increasing concentration of Scar-WA (0, 0.5, 1.7, and 5 µM). (*H*) Histogram of the mean velocity as a function of the functional state of confined cellular extract. (*I*) Schematic of F-actin-based structure and flow within droplet. Scale bars, 10 µm.

ing drastically with observations performed with unperturbed extracts (Movie S3). The dynamics of these networks exhibited two main features: We found in average 40% of the droplets that contained a disorganized meshwork fluctuating erratically as a function of time whereas in 57% of the observations, the patterns were rather static (Fig. 4 *B* and *G* and Fig. S3*C*). Addition of Scar-WA/pWA promotes the formation of dendritic networks that are known to increase the local actin concentration (47). The modulus of elasticity of semi-flexible polymer networks is expected to scale with approximately $(C_A)^{5/2}$, where C_A is the actin concentration (48). This suggests that F-actin network enhanced by Scar-WA/pWA has a larger elasticity than the one generated in absence of Scar nucleators. This stiffness may counterbalance the compressive forces caused by inward flows until it completely impedes them. The homogeneous nucleation of filaments within the droplet space through ScarWA stimulation may counterbalance the importance of F-actin production at the boundary. These results suggest the role of the spatial localization of F-actin production in the formation of symmetry breakings and flow.

Role of Myosin-II on F-actin Flow Dynamics. In unconfined *Xenopus* extract, it has previously been demonstrated that myosin-II activity powered contraction of F-actin meshwork (32). We therefore investigated the role of myosin-II in the establishment of the F-actin symmetry breaking and flow. Myosin II inhibitors, such as blebbistatin (0.1 to 1 mM), ML7 (40 µM), and a Rho-associated kinase (ROCK) inhibitor (Y-27632, 100, or 500 µM), were added alone or in combination within the cell extracts. Interestingly, F-actin flow was persistent in presence of these myosin II inhibitors (Fig. 4*C*). A closer look to the quantification of the F-actin network dynamics in presence of the Rho-kinase inhibitors showed a mean velocity reduced by approximately 30% (Fig. 4*D*). ML7 and blebbistatin also induced slight modifications of the flow dynamics (Fig. S4*A*). We also found that the evolution of the F-actin mesh size as a function of time was modified when myosin inhibitors were added to cell extracts (Fig. S4 *B* and *C*). These data support myosin II participation as force generating elements to the contractile behavior of the F-actin network, but is not crucial in generating F-actin flow. However, they can contribute to the cell polarity determination, as observed for instance during retrograde flux in motile keratocytes (6). Other myosin-like motor proteins could be involved in the F-actin network remodeling.

Role of the Cell-Cycle State on F-actin Flow Dynamics. F-actin dynamics and motor proteins are dependent on the cell cycle states of the oocyte cytoplasm (32). For instance, contractility is abolished in interphase extracts contrary to metaphase extracts (M-phase). Since our experiments were performed in M-phase extracts, we have tested the effect of cell cycle regulation on F-actin dynamics using interphase extracts. We observed F-actin flow dynamics directed inward within confined interphase extracts, with a behavior qualitatively similar to those observed in confined M-phase extracts (Fig. 4*E*). Next, we performed a quantitative analysis of the velocity field of confined interphase extracts and found that the mean velocities were reduced by roughly 40% (Fig. 4*F*; v approximately 54 nm s^{-1}, 10 droplets, approximately 500 trajectories, and five independent experiments). Therefore, in interphase extracts, e.g., in absence of contraction, vectorial F-actin dynamics are still emerging as observed in M-phase extracts, with a reduced velocity.

Discussion

The combination of biochemical perturbations and quantitative image analyses allowed us to examine how confinement induces the generation of symmetry breaking and F-actin flow. Experiments consisting in perturbing actin polymerization or filament nucleation growth lead to the inhibition of F-actin flow process. On the other hand, inhibiting myosin-II activity or changing the cell cycle state of cell extracts did not significantly perturb F-actin flow dynamics in confined environment (Fig. 4*H*). Altogether, these data support the primary role of actin dynamics and nucleation in the generation of F-actin flow. In our experiments, the droplet boundary plays the role of structural anisotropy of the environment by localizing filament growth. Indeed, the confinement geometry provided by the droplets participates in the determination of the final actin steady-state organization.

One hypothesis that may explain the formation of ring-like structures is the ability of F-actin flow to concentrate cytoplasmic components within a restricted area of the droplet. The growth of the ring organization may be correlated with the accretion of actin filaments (Fig. 4*I*). The generation and maintenance of such directional transport of F-actin could involve spatially localized nucleation and actin turnover, such as observed during M-II mouse oocytes and actin retrograde flow of keratocytes and fibroblasts.

Interestingly, our observations evoke F-actin networks involved in physiological functions in oocytes and embryonic systems: maintenance of the spindle asymmetry through cytoplasmic streaming in mouse M-II oocyte (10), chromosome congression and intracellular directional transport in starfish oocyte (12, 13), or pronucleus fusion in *C. elegans* (49).

We anticipate that this assay will be useful to examine cytoplasmic F-actin organization and dynamics involved in oocytes and vertebrate development with a bottom-up approach.

Materials and Methods

Extract-in-Oil Droplet Formations. Extract-in-oil droplet formation was prepared as previously described (26, 34). Briefly, egg PC or the block-polymer PHS-PEO-PHS was first dissolved in mineral oil (0.7 mg/mL and 0.25 mg/mL, respectively). The *Xenopus* CSF egg extracts were added to the mixture of mineral oil/polymer [1% (v CSF/v oil)] at 4 °C. The mixture was gently sheared, by pipetting up and down the solution during few seconds, to generate extract-in-oil droplets (*SI Materials and Methods*).

Imaging. Fluorescence imaging of actin droplets was performed using an Ix81 inverted microscope (Olympus) and a x60 (Plan Apo, NA 1.42) objective, equipped with an electron multiplying charge-coupled device (EM-CCD) camera (C9102 or ImagEM, Hamamatsu Corp., Sewickley, PA). Microscope settings and functions were controlled using SimplePCI software (Hamamatsu). Image analysis was performed using ImageJ (Scion Image), SimplePCI, and MATLAB software programs.

Spatiotemporal Image Tracking and Analysis. We used the Lucas–Kanade feature tracking algorithm in order to extract the specific position of F-actin network (*SI Materials and Methods*). The principle of the Kanade-Lucas Tracking (KLT) algorithm is based on optical flow techniques applied to a small number of features detected in the first image of the sequence.

ACKNOWLEDGMENTS. We acknowledge M.F. Carlier, L. LeGoff, J.F..Joanny, L. Jullien, F. Nedelec, M. Piel, and D. Riveline for discussions and M. Bernot for preliminary experiments. This work was supported by the Centre National de la Recherche Scientifique, the Association pour la Recherche sur le Cancer (SFI20101201426), the Agence Nationale de la Recherche (ANR) (ANR-08-PNANO-050), the Ligue Nationale Contre le Cancer (LNCC)(2009), and Ville de Paris "Emergence" (to Z.G.). B.K.Y. is an LNCC postdoctoral fellow.

1. Pollard TD, Cooper JA (2009) Actin, a central player in cell shape and movement. *Science* 326:1208–1212.
2. Li H, Guo F, Rubinstein B, Li R (2008) Actin-driven chromosomal motility leads to symmetry breaking in mammalian meiotic oocytes. *Nat Cell Biol* 10:1301–1308.
3. Azoury J, et al. (2008) Spindle positioning in mouse oocytes relies on a dynamic meshwork of actin filaments. *Curr Biol* 18:1514–1519.
4. Schuh M, Ellenberg J (2008) A new model for asymmetric spindle positioning in mouse oocytes. *Curr Biol* 18:1986–1992.
5. Pollard TD, Borisy GG (2003) Cellular motility driven by assembly and disassembly of actin filaments. *Cell* 112:453–465.
6. Yam PT, et al. (2007) Actin-myosin network reorganization breaks symmetry at the cell rear to spontaneously initiate polarized cell motility. *J Cell Biol* 178:1207–1221.
7. Martin P, Lewis J (1992) Actin cables and epidermal movement in embryonic wound healing. *Nature* 360:179–183.
8. Mandato CA, Bement WM (2003) Actomyosin transports microtubules and microtubules control actomyosin recruitment during Xenopus oocyte wound healing. *Curr Biol* 13:1096–1105.
9. Clark AG, et al. (2009) Integration of single and multicellular wound responses. *Curr Biol* 19:1389–1395.
10. Yi K, et al. (2011) Dynamic maintenance of asymmetric meiotic spindle position through Arp2/3-complex-driven cytoplasmic streaming in mouse oocytes. *Nat Cell Biol* 13:1252–1258.
11. Field CM, Lenart P (2011) Bulk cytoplasmic actin and its functions in meiosis and mitosis. *Curr Biol* 21:R825–R830.
12. Lenart P, et al. (2005) A contractile nuclear actin network drives chromosome congression in oocytes. *Nature* 436:812–818.
13. Mori M, et al. (2011) Intracellular transport by an anchored homogeneously contracting F-actin meshwork. *Curr Biol* 21:606–611.
14. Mullins RD (2010) Cytoskeletal mechanisms for breaking cellular symmetry. *Cold Spring Harb Perspect Biol* 2:a003392.
15. Paluch E, van der Gucht J, Sykes C (2006) Cracking up: Symmetry breaking in cellular systems. *J Cell Biol* 175:687–692.
16. Blanchoin L, et al. (2000) Direct observation of dendritic actin filament networks nucleated by Arp2/3 complex and WASP/Scar proteins. *Nature* 404:1007–1011.
17. Bernheim-Groswasser A, Wiesner S, Golsteyn RM, Carlier MF, Sykes C (2002) The dynamics of actin-based motility depend on surface parameters. *Nature* 417:308–311.
18. Haviv L, et al. (2006) Reconstitution of the transition from lamellipodium to filopodium in a membrane-free system. *Proc Natl Acad Sci USA* 103:4906–4911.
19. Vignjevic D, et al. (2003) Formation of filopodia-like bundles in vitro from a dendritic network. *J Cell Biol* 160:951–962.
20. Lee K, Gallop JL, Rambani K, Kirschner MW (2010) Self-assembly of filopodia-like structures on supported lipid bilayers. *Science* 329:1341–1345.
21. Claessens MM, Bathe M, Frey E, Bausch AR (2006) Actin-binding proteins sensitively mediate F-actin bundle stiffness. *Nat Mater* 5:748–753.
22. Limozin L, Sackmann E (2002) Polymorphism of cross-linked actin networks in giant vesicles. *Phys Rev Lett* 89:168103.
23. Cosentino Lagomarsino M, et al. (2007) Microtubule organization in three-dimensional confined geometries: Evaluating the role of elasticity through a combined in vitro and modeling approach. *Biophys J* 92:1046–1057.
24. Elbaum M, Kuchnir Fygenson D, Libchaber A (1996) Buckling microtubules in vesicles. *Phys Rev Lett* 76:4078–4081.
25. Pontani LL, et al. (2009) Reconstitution of an actin cortex inside a liposome. *Biophys J* 96:192–198.
26. Pinot M, et al. (2009) Effects of confinement on the self-organization of microtubules and motors. *Curr Biol* 19:954–960.
27. Reymann AC, et al. (2010) Nucleation geometry governs ordered actin networks structures. *Nat Mater* 9:827–832.
28. Desai A, Murray A, Mitchison TJ, Walczak CE (1999) The use of Xenopus egg extracts to study mitotic spindle assembly and function in vitro. *Methods Cell Biol* 61:385–412.
29. Heald R, Tournebize R, Habermann A, Karsenti E, Hyman A (1997) Spindle assembly in Xenopus egg extracts: Respective roles of centrosomes and microtubule self-organization. *J Cell Biol* 138:615–628.
30. Gaetz J, Gueroui Z, Libchaber A, Kapoor TM (2006) Examining how the spatial organization of chromatin signals influences metaphase spindle assembly. *Nat Cell Biol* 8:924–932.
31. Waterman-Storer C, et al. (2000) Microtubules remodel actomyosin networks in Xenopus egg extracts via two mechanisms of F-actin transport. *J Cell Biol* 150:361–376.
32. Field CM, et al. (2011) Actin behavior in bulk cytoplasm is cell cycle regulated in early vertebrate embryos. *J Cell Sci* 124:2086–2095.
33. Liu AP, Fletcher DA (2009) Biology under construction: In vitro reconstitution of cellular function. *Nat Rev Mol Cell Biol* 10:644–650.
34. Jimenez AM, et al. (2011) Towards high throughput production of artificial egg oocytes using microfluidics. *Lab Chip* 11:429–434.
35. Zhang W, Robinson DN (2005) Balance of actively generated contractile and resistive forces controls cytokinesis dynamics. *Proc Natl Acad Sci USA* 102:7186–7191.
36. Rankin S, Kirschner MW (1997) The surface contraction waves of Xenopus eggs reflect the metachronous cell-cycle state of the cytoplasm. *Curr Biol* 7:451–454.
37. Vicker MG (2002) F-actin assembly in Dictyostelium cell locomotion and shape oscillations propagates as a self-organized reaction-diffusion wave. *FEBS Lett* 510:5–9.
38. Gerisch G, et al. (2004) Mobile actin clusters and traveling waves in cells recovering from actin depolymerization. *Biophys J* 87:3493–3503.
39. Weiner OD, Marganski WA, Wu LF, Altschuler SJ, Kirschner MW (2007) An actin-based wave generator organizes cell motility. *PLoS Biol* 5:e221.
40. Levayer R, Lecuit T (2011) Biomechanical regulation of contractility: spatial control and dynamics. *Trends Cell Biol* 22:61–81.
41. Boukellal H, Campás O, Joanny JF, Prost J, Sykes C (2004) Soft Listeria: Actin-based propulsion of liquid drops. *Phys Rev E Stat Nonlin Soft Matter Phys* 69:061906.
42. Carlsson AE (2010) Dendritic actin filament nucleation causes traveling waves and patches. *Phys Rev Lett* 104:228102.
43. Misteli T (2001) The concept of self-organization in cellular architecture. *J Cell Biol* 155:181–185.
44. Karsenti E (2008) Self-organization in cell biology: A brief history. *Nat Rev Mol Cell Biol* 9:255–262.
45. Gatlin JC, et al. (2009) Spindle fusion requires dynein-mediated sliding of oppositely oriented microtubules. *Curr Biol* 19:287–296.
46. Machesky LM, et al. (1999) Scar, a WASp-related protein, activates nucleation of actin filaments by the Arp2/3 complex. *Proc Natl Acad Sci USA* 96:3739–3744.
47. Pollard TD, Blanchoin L, Mullins RD (2000) Molecular mechanisms controlling actin filament dynamics in nonmuscle cells. *Annu Rev Biophys Biomol Struct* 29:545–576.
48. MacKintosh FC, Kas J, Janmey PA (1995) Elasticity of semiflexible biopolymer networks. *Phys Rev Lett* 75:4425–4428.
49. Xiong H, Mohler WA, Soto MC (2011) The branched actin nucleator Arp2/3 promotes nuclear migrations and cell polarity in the *C. elegans* zygote.. *Dev Biol* 357:356–369.